



Published in final edited form as:

*Mol Pharm.* 2020 August 03; 17(8): 3140–3147. doi:10.1021/acs.molpharmaceut.0c00437.

## A Molecularly Targeted Intraoperative Near-Infrared Fluorescence Imaging Agent for High Grade Serous Ovarian Cancer

Kimberly Fung<sup>1,2,†</sup>, Sai Kiran Sharma<sup>3,4,†</sup>, Outi Keinänen<sup>1,3</sup>, Kara Long Roche<sup>5</sup>, Jason S. Lewis<sup>3,4</sup>, Brian M. Zeglis<sup>1,2,3,\*</sup>

<sup>1</sup>Department of Chemistry, Hunter College, City University of New York, New York, NY, 10028, United States

<sup>2</sup>Ph.D. Program in Chemistry, The Graduate Center of the City University of New York, New York, NY, 10016, United States

<sup>3</sup>Department of Radiology, Memorial Sloan Kettering Cancer Center, New York, NY, 10065, United States

<sup>4</sup>Program in Molecular Pharmacology, Memorial Sloan Kettering Cancer Center, New York, NY, 10065, United States

<sup>5</sup>Department of Surgery, Memorial Sloan Kettering Cancer Center, New York, NY, 10065, United States

### Abstract

Ovarian cancer is the fifth leading cause of cancer deaths amongst women, accounting for more deaths than any other cancer of the female reproductive system. The foundation of its management consists of cytoreductive surgery (CRS) followed by systemic chemotherapy, with the completeness of surgical resection consistently identified as one of the most important prognostic factors for the disease. The goal of our investigation is the development of a near-infrared fluorescence (NIRF) imaging agent for the intraoperative imaging of high-grade serous ovarian cancer (HGSOC). As surgeons are currently limited to the visual and manual assessment of tumor tissue during CRS, this technology could facilitate more complete resections as well as serve important functions at other points in the surgical management of the disease. Elevated levels of

\*Corresponding Author: Brian M. Zeglis. 413 East 69<sup>th</sup> Street, New York, NY, 10021. Phone: 212-896-0433. Fax: 212-772-5332. bz102@hunter.cuny.edu.

#### Author Contributions

The manuscript was written with contributions from all of the authors. All authors have given approval to the final version of the manuscript.

<sup>†</sup>These two authors contributed equally to this work.

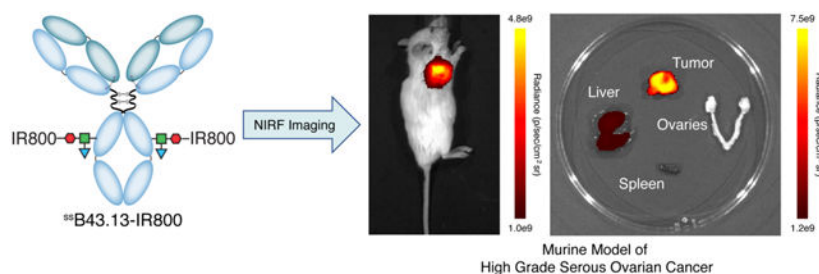
All animals were treated according to guidelines approved by the Research Animal Resource Center and the Institutional Animal Care and Use Committee at Memorial Sloan Kettering Cancer Center. The authors declare no competing financial interest.

#### Supporting Information

The Supporting Information is available free of charge on the ACS Publications website at DOI: <https://pubs.acs.org/doi/10.1021/acs.molpharmaceut.0c00437>. Reagents and general procedures; detailed experimental methods for chemical syntheses, *in vitro* experiments, *in vivo* experiments, and immunohistochemical staining; SDS-PAGE of <sup>55</sup>B43.13-IR800; flow cytometry data; fluorescence microscopy data; *in vivo* and *ex vivo* NIRF images; and immunohistochemical staining of primary tumor and lymph node samples from a patient with clear cell ovarian cancer.

cancer antigen 125 (CA125) have proven a useful biomarker of HGSOC, and the CA125-targeting antibody B43.13 has shown potential as a platform for immunoPET imaging in murine models of ovarian cancer. Herein, we report the development of a NIRF imaging agent based on B43.13:  $^{88}\text{B43.13-IR800}$ . We site-specifically modified the heavy chain glycans of B43.13 with the near-infrared dye IRDye<sup>®</sup> 800CW using a chemoenzymatic approach developed in our laboratories. SDS-PAGE analysis confirmed the specificity of the conjugation reaction, and flow cytometry, immunostaining, and fluorescence microscopy verified the specific binding of  $^{88}\text{B43.13-IR800}$  to CA125-expressing OVCAR3 human ovarian cancer cells. NIRF imaging studies demonstrated that  $^{88}\text{B43.13-IR800}$  can be used to image CA125-expressing HGSOC tumors in subcutaneous, orthotopic, and patient-derived xenograft mouse models. Finally, *ex vivo* analyses confirmed that  $^{88}\text{B43.13-IR800}$  can bind and identify CA125-expressing cells in primary tumor and metastatic lymph node samples from human patients with HGSOC.

## GRAPHICAL ABSTRACT



## Keywords

B43.13; IR800CWDye; CA125; ovarian cancer; site-specific bioconjugation; near-infrared fluorescence imaging; immunoconjugate

## INTRODUCTION

Ovarian cancer is the most lethal gynecologic malignancy and the fifth leading cause of cancer-related deaths in women.<sup>1</sup> Cytoreductive surgery (CRS) remains the most effective first-line treatment for the disease. However, the complete removal of malignant tissue during surgery can be extremely challenging. In patients with unresectable disease, neoadjuvant chemotherapy followed by interval CRS is a valid alternative to primary CRS and is supported by multicenter randomized controlled trials.<sup>2–4</sup> The volume of residual disease (RD) after CRS is one of the strongest prognostic indicators of progression-free and overall survival in ovarian cancer patients.<sup>5</sup> While optimal CRS is defined as RD <1 cm, each incremental decrease in RD below 1 cm improves outcomes.<sup>2, 3</sup> In spite of this, the determination of RD is based solely on the surgeon's visual and manual assessment. The limitations of this approach are underscored by a study that discovered high inter-observer variability, with surgeons more often *underestimating* rather than *overestimating* the amount of RD.<sup>6</sup> Furthermore, several studies have examined the value of postoperative CT and found that anatomical imaging revealed RD >1 cm in up to 40% of patients that had been deemed 'optimally resected'.<sup>7, 8</sup> Collectively, this makes a clear case for improving the

intraoperative assessment and accurate reporting of RD in the treatment of ovarian cancer patients. Therefore, the development of tools that can improve the assessment of RD during CRS is a vitally important unmet clinical need. The development of this technology could aid clinicians in achieving greater reductions in disease burden via the NIRF-guided resection of residual tumor tissue, thereby improving patient outcomes.

High-grade serous ovarian cancer (HGSOC) comprises the vast majority (~70%) of ovarian adenocarcinomas.<sup>9</sup> A vital molecular signature of this malignant histotype is the over-expression of MUC16, a mucinous glycoprotein that carries the cancer antigen 125 (CA125) epitope.<sup>10, 11</sup> A telltale sign of ovarian cancer is elevated serum CA125 levels, and malignant cells themselves are known to profusely express this tumor-associated antigen.<sup>12</sup> Despite being a shed antigen, high concentrations of MUC16/CA125 remain on the surface of cancer cells, enabling the PET imaging of ovarian cancer.<sup>13</sup> A CA125-targeted intraoperative imaging agent could thus be a valuable surgical tool for the identification of microscopic or metastatic deposits within the peritoneum and in clinically normal-appearing lymph nodes. While advanced HGSOC is the most commonly encountered form of ovarian cancer and thus the most appropriate malignancy in which to study this technology, rarer subtypes of epithelial ovarian cancer — such as endometrioid, clear cell, and low grade serous carcinomas — may benefit from this approach as well and will be incorporated into future work once its clinical utility has been established.

We recently reported the creation of a PET imaging agent for the *in vivo* delineation of CA125 expression in ovarian cancer based on B43.13, a CA125-targeting murine antibody ( $K_D$  for CA125 = 1.2 nM) formerly tested as a immunotherapeutic and a radiotracer for immunoscintigraphy in ovarian cancer patients.<sup>14</sup> Under the name oregovomab, B43.13 continues to be investigated in clinical trials as part of combination treatments for epithelial ovarian cancer alongside chemotherapy and immunotherapy.<sup>15–22</sup> In addition, in our hands, B43.13-based radioimmunoconjugates labeled with [<sup>64</sup>Cu]Cu<sup>2+</sup> and [<sup>89</sup>Zr]Zr<sup>4+</sup> have demonstrated promise for the PET imaging of CA125 expression in murine xenograft models of human ovarian cancer.<sup>13, 14</sup> *In vivo* imaging experiments in murine xenograft models of HGSOC clearly demonstrate that [<sup>89</sup>Zr]Zr-DFO-B43.13 is not only capable of visualizing primary tumor tissue but also can provide sensitive maps of the metastatic spread of ovarian cancer through the ipsilateral chain of lymph nodes.<sup>14</sup>

Herein, we report the development of <sup>88</sup>B43.13-IR800, a CA125-targeting molecular probe for the NIRF imaging of HGSOC during CRS. To this end, a pair of fluorophore-labeled immunoconjugates — <sup>88</sup>B43.13-AF488 and <sup>88</sup>B43.13-IR800 — were synthesized via the chemoenzymatic bioconjugation of Alexa Fluor<sup>™</sup> 488 (AF488) and IRDye<sup>®</sup> 800CW (IR800) to the heavy chain glycans of B43.13. After employing <sup>88</sup>B43.13-AF488 for *in vitro* characterization assays, near-infrared fluorescence imaging experiments were performed with <sup>88</sup>B43.13-IR800 in mice bearing subcutaneous, orthotopic, and patient-derived xenograft mouse models of HGSOC. Finally, the translational potential of <sup>88</sup>B43.13-IR800 was further examined via the *ex vivo* histopathological staining of primary tumor and metastatic lymph node tissue samples obtained from HGSOC patients that underwent CRS.

It is important to note that we are not the first to propose creating an intraoperative imaging agent for ovarian cancer. Indeed, a Phase II clinical trial focused on the use of OTL38 — a fluorophore-modified variant of folate that targets folate-receptor alpha (FOLR1) — for intraoperative imaging during CRS has recently produced promising results.<sup>23, 24</sup> In addition, the use of indocyanine green (ICG), a non-targeted fluorophore, has been explored in a small clinical trial, though high false positive results were observed.<sup>25</sup> A handful of preclinical reports investigating the potential of nanoparticle-based imaging agents for the NIRF imaging of ovarian cancer have also recently been published.<sup>26, 27</sup> Nonetheless, we contend that the CA125-targeted strategy we discuss here will offer an improvement over these strategies for three reasons. First, targeted imaging agents generally offer greater sensitivity and specificity than untargeted probes that rely upon the enhanced permeability and retention effect for accumulation in tumor tissue. Second, targeting an ovarian cancer-specific biomarker (*i.e.* CA125) rather than an antigen with significant levels of expression in healthy tissues (*e.g.* FOLR1) will further bolster the sensitivity and specificity of the imaging agent and yield improved tumor-to-background ratios that will translate into higher contrast visualization of metastatic tumor nodules in the peritoneal cavity. And third, the remarkable ability of B43.13-based probes to delineate small deposits of metastatic disease within lymph nodes — as illustrated via immunoPET — could prove highly valuable in the surgical setting, particularly in the context of clinically normal-appearing nodes, for which there is currently no consensus for management.<sup>14</sup>

## RESULTS AND DISCUSSION

The first step in the investigation was the attachment of Alexa Fluor™ 488 (AF488) and IRDye® 800CW (IR800) to the CA125-targeting antibody. To this end, we turned to a chemoenzymatic approach to bioconjugation developed by our laboratories that leverages a pair of enzymes and strain-promoted azide-alkyne click chemistry to append cargoes to the heavy chain glycans of the antibody's Fc region.<sup>28–30</sup> This strategy is predicated on three steps: (1) the truncation of the heavy chain glycans with EndoS, an enzyme which cleaves off most of each oligosaccharide chain and leaves only a single GlcNAc residue; (2) the use of a promiscuous galactosyltransferase — [GalT-(Y289L)] — to incorporate N<sub>3</sub>-bearing galactose sugars (GalNAz) into the glycans; and (3) the click ligation between the azide-modified antibody and dibenzocyclooctyne (DBCO)-bearing variants of AF488 or IR800 (Figure 1A). We have demonstrated that this strategy produces better defined and more homogenous immunoconjugates with improved *in vivo* performance compared to constructs created using random lysine-based bioconjugation methods.<sup>31–35</sup> In this case, this methodology produces <sup>ss</sup>B43.13-AF488 and <sup>ss</sup>B43.13-IR800 immunoconjugates with degrees of labeling of ~1.0 and ~0.75 fluorophores/mAb, respectively. While these values admittedly lie below the theoretical maximum of 2 fluorophores/mAb, they are consistent with previous results obtained using this strategy in conjunction with bulky, hydrophobic fluorophores.<sup>32, 34</sup> Denaturing SDS-PAGE was employed to confirm the site-specificity of the modification procedure and clearly illustrates that the chemoenzymatic manipulation of the antibody alters the heavy chain while leaving the light chain untouched (Supplementary Figure S1).

*In vitro* characterization experiments were performed using <sup>88</sup>B43.13-AF488 due to the compatibility of its excitation and emission wavelengths with flow cytometry instruments and fluorescence microscopes. More specifically, flow cytometry experiments with both CA125-positive (OVCAR3) and CA125-negative (SKOV3) human ovarian cancer cells confirmed the specificity of the immunoconjugate by demonstrating binding to the former but not the latter (Figure 1B and Supplemental Figure S2). Furthermore, the specificity of the probe was illustrated in fluorescence microscopy experiments, which clearly showed <sup>88</sup>B43.13-AF488 binding to OVCAR3 cells but not SKOV3 cells (Figure 1C and Supplemental Figure S2).

Due to the enhanced tissue penetration of near-infrared light, intraoperative imaging agents bearing near-infrared fluorophores are more viable candidates for clinical translation than their shorter wavelength cousins. Consequently, <sup>88</sup>B43.13-IR800 was employed for all of the *in vivo* validation experiments of the investigation. Along these lines, preliminary NIRF imaging was performed in athymic nude mice bearing subcutaneous CA125-positive OVCAR3 xenografts. We previously observed that [<sup>89</sup>Zr]Zr-DFO-B43.13 reaches a near-optimal biodistribution in tumor-bearing mice 72 h after its administration, so this interval was chosen for all experiments with <sup>88</sup>B43.13-IR800; however, slightly longer circulation times (*e.g.* 96, 120, or 144 h) could undoubtedly be used in the clinical setting without compromising the performance of the immunoconjugate. Moving on to the data, high levels of accretion of <sup>88</sup>B43.13-IR800 were observed in tumor tissue (Supplementary Figure S4). Interestingly, in some — but not all — of the mice, NIRF signal was observed in the lymph nodes adjacent to the tumor. Our previous experience with [<sup>89</sup>Zr]Zr-DFO-B43.13 immunoPET in OVCAR3-bearing nude mice suggests that this NIRF signal stems from the uptake of the immunoconjugate in metastatic lesions within the ipsilateral lymph node chain. While the concentration of the immunoconjugate in most healthy organs remains low, significant background uptake was observed in the liver. This accumulation likely arises from either (a) the formation of immune complexes with shed CA125 in the blood and their subsequent deposition in the liver *or* (b) the clearance of the exogenously administered murine IgG1 (*i.e.* <sup>88</sup>B43.13-IR800) by hepatocytes or resident macrophages (Kupffer cells) in the liver.

Next, the NIRF imaging and post-mortem resection of athymic nude mice bearing *orthotopic* OVCAR3 xenografts implanted in the left ovary provided an opportunity to simulate the use of <sup>88</sup>B43-IR800 for intraoperative imaging (Figure 2 and Supplemental Figure S5). In a representative mouse, NIRF imaging during necropsy revealed high levels of fluorescence in the liver and left ovary. Upon further resection, significant uptake of <sup>88</sup>B43.13-IR800 was detected in these two tissues as well as a peritoneal implant and the renal lymph nodes. The ipsilateral and contralateral inguinal lymph nodes, in contrast, did not contain significant NIRF signal. Subsequent histopathologic analysis of the resected tissues identified the primary tumor in the left ovary and confirmed the presence of neoplastic cells in both the peritoneal implant and the renal lymph nodes. Critically, however, the inguinal lymph nodes that did not produce signal during *ex vivo* NIRF imaging proved negative for the presence of neoplastic cells upon histopathological analysis.

These promising preliminary results prompted us to explore the performance of <sup>88</sup>B43.13-IR800 in Nod-Scid-Gamma (NSG) mice bearing subcutaneous, orthotopic, and patient-derived xenograft (PDX) models of HGSOc. This switch to NSG mice was made in response to the low take-rate, slow growth, and inconsistent size of OVCAR3 xenografts in athymic nude mice. In contrast, the absence of functional NK cells in the highly immunocompromised NSG mice allows for a nearly 100% take-rate of OVCAR3 xenografts. Furthermore, NSG mice are a preferred strain for the propagation of frozen parent PDX tumor seeds to generate larger cohorts of PDX-bearing mice for preclinical imaging. Our first *in vivo* experiments with NSG mice employed our most basic tumor model: subcutaneous xenografts (Figure 3). In these mice, higher levels of NIRF signal were observed with <sup>88</sup>B43.13-IR800 compared to mIgG-IR800, a non-specific, isotype-control immunoconjugate. This observation was supported by *ex vivo* imaging, which likewise revealed significantly higher uptake of <sup>88</sup>B43.13-IR800 in the tumor compared to the negative control. In the <sup>88</sup>B43.13-IR800-treated mice, very little NIRF signal was observed in the healthy organs — including, critically, the ovaries — with the exception of the liver, which again displayed moderate uptake of the immunoconjugate.

We next turned to orthotopic and patient-derived xenografts (PDX) to provide more realistic recapitulations of human disease. In NSG mice bearing orthotopic OVCAR3 tumors and subcutaneous, CA125-positive PDXs, dramatically higher levels of NIRF signal were observed with <sup>88</sup>B43.13-IR800 compared to mIgG-IR800 (Figure 4 and Supplemental Figure S6). In these mice, the uptake of <sup>88</sup>B43.13-IR800 in most healthy organs remains low, but elevated NIRF signal was again observed in the liver. Before moving on, it is worth noting that while moderate liver uptake was observed in each of the NSG models tested, the hepatic NIRF signal was substantially higher in the athymic nude mice in which the original pilot studies were performed. This discrepancy may stem from strain-induced differences in the catabolism of exogenously introduced murine IgG1, but it also may be a result of the higher mass of <sup>88</sup>B43.13-IR800 employed in the nude mice (100 µg) compared to the NSG mice (50 µg). These data underscore the need to determine an optimized dose of <sup>88</sup>B43.13-IR800 for clinical studies that will facilitate target-mediated clearance of the NIRF probe by tumors in the peritoneum whilst yielding high contrast signal for the surgeons performing CRS.

Finally, in order to further probe the translational promise of <sup>88</sup>B43.13-IR800, the fluorophore-bearing immunoconjugate was tested with tissue sections obtained from tumors and metastatic lymph nodes harvested during the surgical debulking of patients with HGSOc at Memorial Sloan Kettering Cancer Center (Figure 5). Manual immunohistochemical analysis of adjacent sections of these tissues with unmodified B43.13, <sup>88</sup>B43.13-IR800, and a commercially-available anti-CA125 antibody produced identical staining patterns for CA125 expression. On the other hand, tissues from a patient with CA125-negative tumors — clear cell carcinoma of the ovary — stained negative with all three antibodies (Supplementary Figure S7). Taken together, these results suggest that the bioconjugation of B43.13 does not significantly hinder its ability to bind and identify CA125-expressing cells in human patients, thereby making a strong case for clinical translation.

## CONCLUSION

In this investigation, we explored the utility of <sup>88</sup>B43.13-IR800 for the intraoperative near-infrared imaging of CA125-expressing high-grade serous ovarian cancer (HGSOC) tumors. The ability of <sup>88</sup>B43.13-IR800 to delineate both primary tumor tissue and metastatic lesions from healthy organs in subcutaneous, orthotopic, and patient-derived xenograft mouse models of HGSOC was clearly demonstrated. Furthermore, <sup>88</sup>B43.13-IR800 proved capable of staining primary tumors and metastatic lymph nodes in clinically resected samples from human HGSOC patients. In light of these data, we are optimistic that the clinical translation of <sup>88</sup>B43.13-IR800 could help surgeons performing CRS achieve the most complete resection of disease, thereby further reducing the volume of residual disease present after surgery and improving the outcomes of patients with HGSOC.

## Supplementary Material

Refer to Web version on PubMed Central for supplementary material.

## Acknowledgment

The authors are grateful to Dr. Madi Madiyalakan and Oncoquest Inc. for providing the B43.13 antibody.

### Funding Sources

National Institutes of Health (R01 CA240963, U01 CA221046, R01 CA204167, R35 CA232130, and P30 CA008748); the Tow Foundation; the MSK Center for Molecular Imaging & Nanotechnology; the MSK Imaging and Radiation Sciences Program; and the MSK Molecularly Targeted Intraoperative Imaging Fund.

## Abbreviations

<b>CA125</b>	cancer antigen 125
<b>HGSOC</b>	high grade serous ovarian cancer
<b>CRS</b>	cytoreductive surgery
<b>RD</b>	residual disease
<b>NIRF</b>	near-infrared fluorescence
<b>PET</b>	positron emission tomography
<b>ICG</b>	indocyanine green
<b>AF488</b>	Alexa Fluor™ 488
<b>IR800</b>	IRDye® 800CW
<b>PAGE</b>	polyacrylamide gel electrophoresis
<b>DBCO</b>	dibenzocyclooctyne
<b>NSG</b>	Nod-Scid-Gamma
<b>PDX</b>	patient-derived xenograft

## References

1. Siegel RL; Miller KD; Jemal A, Cancer statistics, 2020. *CA Cancer J. Clin* 2020, 70 (1), 7–30. [PubMed: 31912902]
2. van der Burg MEL; van Lent M; Buyse M; Kobierska A; Colombo N; Favalli G; Lacave AJ; Nardi M; Renard J; Pecorelli S, The effect of debulking surgery after induction chemotherapy on the prognosis in advanced epithelial ovarian cancer. *New Engl. J. Med* 1995, 332 (10), 629–634. [PubMed: 7845426]
3. Vergote I; Tropé CG; Amant F; Kristensen GB; Ehlen T; Johnson N; Verheijen RHM; van der Burg MEL; Lacave AJ; Panici PB; Kenter GG; Casado A; Mendiola C; Coens C; Verleye L; Stuart GCE; Pecorelli S; Reed NS, Neoadjuvant chemotherapy or primary surgery in stage IIIC or IV ovarian cancer. *New Engl. J. Med* 2010, 363 (10), 943–953. [PubMed: 20818904]
4. Wright AA; Bohlke K; Armstrong DK; Bookman MA; Cliby WA; Coleman RL; Dizon DS; Kash JJ; Meyer LA; Moore KN; Olawaiye AB; Oldham J; Salani R; Sparacio D; Tew WP; Vergote I; Edelson MI, Neoadjuvant chemotherapy for newly diagnosed, advanced ovarian cancer: Society of gynecologic oncology and american society of clinical oncology clinical practice guideline. *J. Clin. Oncol* 2016, 34 (28), 3460–3473. [PubMed: 27502591]
5. Chi DS; Liao JB; Leon LF; Venkatraman ES; Hensley ML; Bhaskaran D; Hoskins WJ, Identification of prognostic factors in advanced epithelial ovarian carcinoma. *Gynecol. Oncol* 2001, 82 (3), 532–537. [PubMed: 11520151]
6. Préfontaine M; Gelfand AT; Donovan JT; Powell JL, Reproducibility of tumor measurements in ovarian cancer: A study of interobserver variability. *Gynecol. Oncol* 1994, 55 (1), 87–90. [PubMed: 7959274]
7. Sala E; Mannelli L; Yamamoto K; Griffin M; Griffin N; Grant L; Parker R; Crawford R, The value of postoperative/preadjuvant chemotherapy computed tomography in the management of patients with ovarian cancer. *Int. J. Gynecol. Cancer* 2011, 21 (2), 296. [PubMed: 21721161]
8. Lakhman Y; Akin O; Sohn MJ; Zheng J; Moskowitz CS; Iyer RB; Barakat RR; Sabbatini PJ; Chi DS; Hricak H, Early postoperative CT as a prognostic biomarker in patients with advanced ovarian, tubal, and primary peritoneal cancer deemed optimally debulked at primary cytoreductive surgery. *Am. J. Roentgenol* 2012, 198 (6), 1453–1459. [PubMed: 22623562]
9. Mutch DG; Prat J, 2014 FIGO staging for ovarian, fallopian tube and peritoneal cancer. *Gynecol. Oncol* 2014, 133 (3), 401–404. [PubMed: 24878391]
10. Davis HM; Zurawski VR; Bast RC; Klug TL, Characterization of the CA 125 Antigen associated with human epithelial ovarian carcinomas. *Cancer Res.* 1986, 46 (12 Part 1), 6143. [PubMed: 2430690]
11. Yin BWT; Dnistrian A; Lloyd KO, Ovarian cancer antigen CA125 is encoded by the MUC16 mucin gene. *Int. J. Cancer* 2002, 98 (5), 737–740. [PubMed: 11920644]
12. Felder M; Kapur A; Gonzalez-Bosquet J; Horibata S; Heintz J; Albrecht R; Fass L; Kaur J; Hu K; Shojaei H; Whelan RJ; Patankar MS, MUC16 (CA125): Tumor biomarker to cancer therapy, a work in progress. *Mol. Cancer* 2014, 13 (1), 129. [PubMed: 24886523]
13. Sharma SK; Wuest M; Wang M; Glubrecht D; Andrais B; Lapi SE; Wuest F, Immuno-PET of epithelial ovarian cancer: Harnessing the potential of CA125 for non-invasive imaging. *Eur. J. Nucl. Med. Mol. Imag. Res* 2014, 4 (1), 60.
14. Sharma SK; Sevak KK; Monette S; Carlin SD; Knight JC; Wuest FR; Sala E; Zeglis BM; Lewis JS, Preclinical <sup>89</sup>Zr immuno-PET of high-grade serous ovarian cancer and lymph node metastasis. *J. Nucl. Med* 2016, 57 (5), 771–776. [PubMed: 26837339]
15. Hisatsune A; Nakayama H; Kawasaki M; Horie I; Miyata T; Isohama Y; Kim KC; Katsuki H, Anti-MUC1 antibody inhibits EGF receptor signaling in cancer cells. *Biochem. Biophys. Res. Commun* 2011, 405 (3), 377–381. [PubMed: 21219855]
16. McQuarrie SA; Baum RP; Niesen A; Madiyalakan R; Korz W; Sykes TR; Sykes CJ; Hör G; McEwan AJ; Noujaim AA, Pharmacokinetics and radiation dosimetry of <sup>99</sup>Tcm-labelled monoclonal antibody B43.13 in ovarian cancer patients. *Nucl. Med. Commun* 1997, 18 (9), 878–886. [PubMed: 9352556]

17. Schultes BC; Baum RP; Niesen A; Noujaim AA; Madiyalakan R, Anti-idiotype induction therapy: Anti-CA125 antibodies (Ab<sub>3</sub>) mediated tumor killing in patients treated with Ovarex mAb B43.13 (Ab<sub>1</sub>). *Cancer Immunol. Immunother* 1998, 46 (4), 201–212. [PubMed: 9671143]
18. Noujaim AA; Schultes BC; Baum RP; Madiyalakan R, Induction of CA125-specific B and T cell responses in patients injected with MAb-B43.13—Evidence for antibody-mediated antigen-processing and presentation of CA125 in vivo. *Cancer Biother. Radiopharm* 2001, 16 (3), 187–203. [PubMed: 11471484]
19. Gordon AN; Schultes BC; Gallion H; Edwards R; Whiteside TL; Cermak JM; Nicodemus CF, CA125- and tumor-specific T-cell responses correlate with prolonged survival in oregovomab-treated recurrent ovarian cancer patients. *Gynecol. Oncol* 2004, 94 (2), 340–351. [PubMed: 15297171]
20. Salouti M; Babaei MH; Rajabi H; Rasaei MJ, Preparation and biological evaluation of <sup>177</sup>Lu conjugation PR81 for radioimmunotherapy of breast cancer. *Nucl. Med. Biol* 2011, 38, 849–855. [PubMed: 21843781]
21. Hughes ODM; Bishop MC; Perkins AC; Frier M; Price MR; Denton G; Smith A; Rutherford R; Schubiger PA, Preclinical evaluation of copper-67 labelled anti-MUC1 mucin antibody C595 for therapeutic use in bladder cancer. *Eur. J. Nucl. Med* 1997, 24 (4), 439–443. [PubMed: 9096097]
22. Brewer M; Angioli R; Scambia G; Lorusso D; Terranova C; Panici PB; Raspagliesi F; Scollo P; Plotti F; Ferrandina G; Salutati V; Ricci C; Braly P; Holloway R; Method M; Madiyalakan M; Bayever E; Nicodemus C, Front-line chemo-immunotherapy with carboplatin-paclitaxel using oregovomab indirect immunization in advanced ovarian cancer: A randomized Phase II study. *Gynecol. Oncol* 2020, 156, 523–529. [PubMed: 31916979]
23. Randall LM; Wenham RM; Low PS; Dowdy SC; Tanyi JL, A phase II, multicenter, open-label trial of OTL38 injection for the intra-operative imaging of folate receptor-alpha positive ovarian cancer. *Gynecol. Oncol* 2019, 155 (1), 63–68. [PubMed: 31362825]
24. Hoogstins CE; Tummers QR; Gaarenstroom KN; de Kroon CD; Trimbos JB; Bosse T; Smit VT; Vuyk J; van de Velde CJ; Cohen AF; Low PS; Burggraaf J; Vahrmeijer AL, A novel tumor-specific agent for intraoperative near-infrared fluorescence imaging: A translational study in healthy volunteers and patients with ovarian cancer. *Clin. Cancer. Res* 2016, 22 (12), 2929–2938. [PubMed: 27306792]
25. Tummers QR; Hoogstins CE; Peters AA; de Kroon CD; Trimbos JB; van de Velder CJ; Frangioni JV; Vahrmeijer AL; Gaarenstroom KN, The value of intraoperative near-infrared fluorescence imaging based on enhanced permeability and retention of indocyanine green: feasibility and false-positives in ovarian cancer. *PLoS One* 2015, 2015 (6), e0129766.
26. Wang P; Fan Y; Lu L; Liu L; Fan L; Zhao M; Xie Y; Xu C; Zhang F, NIR-II nanoprobe in-vivo assembly to improve image-guided surgery for metastatic ovarian cancer. *Nat. Commun* 2018, 9, 2898. [PubMed: 30042434]
27. Ceppi L; Bardhan NM; Na YJ; Seigel A; Rajan N; Fruscio R; M. G. DC; Belcher AM; Birrer MJ, Real-time single-walled carbon nanotube-based fluorescence imaging improves survival after debulking surgery in an ovarian cancer model. *ACS Nano* 2019, 13 (5), 5356–5365. [PubMed: 31009198]
28. Zeglis BM; Davis CB; Abdel-Atti D; Carlin SD; Chen A; Aggeler R; Agnew BJ; Lewis JS, Chemoenzymatic strategy for the synthesis of site-specifically labeled immunoconjugates for multimodal PET and optical imaging. *Bioconj. Chem* 2014, 25 (12), 2123–2128.
29. Zeglis BM; Davis CB; Aggeler R; Kang HC; Chen A; Agnew BJ; Lewis JS, Enzyme-mediated methodology for the site-specific radiolabeling of antibodies based on catalyst-free click chemistry. *Bioconj. Chem* 2013, 24 (6), 1057–1067.
30. Adumeau P; Sharma SK; Brent C; Zeglis BM, Site-specifically labeled immunoconjugates for molecular imaging—Part 1: Cysteine residues and glycans. *Mol. Imag. Biol* 2016, 18 (1), 1–17.
31. Vivier D; Fung K; Rodriguez C; Adumeau P; Ulaner GA; Lewis JS; Sharma SK; Zeglis BM, The influence of glycans-specific bioconjugation on the Fc[γ]RI binding and in vivo performance of <sup>89</sup>Zr-DFO-pertuzumab. *Theranostics* 2020, 10 (4), 1746–1757. [PubMed: 32042334]
32. Houghton JL; Zeglis BM; Abdel-Atti D; Aggeler R; Sawada R; Agnew BJ; Scholz WW; Lewis JS, Site-specifically labeled CA19.9-targeted immunoconjugates for the PET, NIRF, and multimodal

PET/NIRF imaging of pancreatic cancer. *Proc. Natl. Acad. Sci. U. S. A* 2015, 112 (52), 15850. [PubMed: 26668398]

33. Cook BE; Adumeau P; Membreno R; Carnazza KE; Brand C; Reiner T; Agnew BJ; Lewis JS; Zeglis BM, Pretargeted PET imaging using a site-specifically labeled immunoconjugate. *Bioconj. Chem* 2016, 27 (8), 1789–1795.
34. Adumeau P; Carnazza KE; Brand C; Carlin SD; Reiner T; Agnew BJ; Lewis JS; Zeglis BM, A pretargeted approach for the multimodal PET/NIRF imaging of colorectal cancer. *Theranostics* 2016, 6 (12), 2267–2277. [PubMed: 27924162]
35. Adumeau P; Vivier D; Sharma SK; Wang J; Zhang T; Chen A; Agnew BJ; Zeglis BM, Site-specifically labeled antibody-drug conjugate for simultaneous therapy and immunoPET. *Mol. Pharm* 2018, 15, 892–898. [PubMed: 29356543]

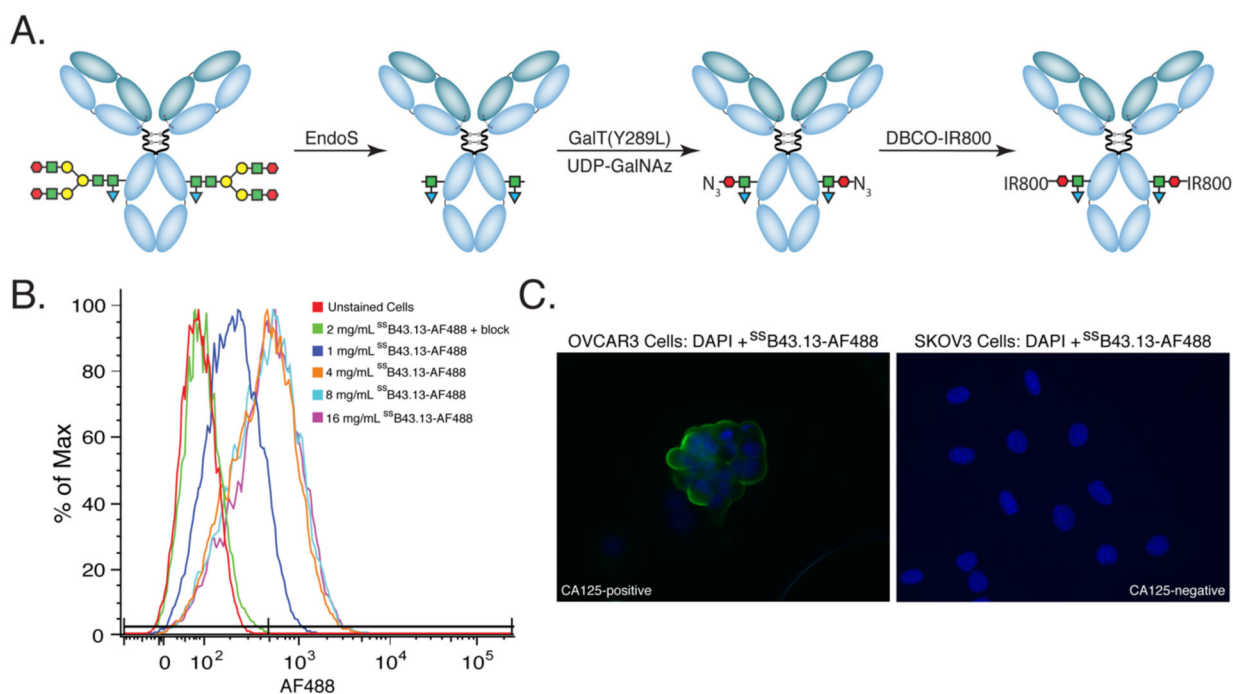


**Figure 1. The synthesis and biological characterization of  $^{ss}B43.13-IR800$ .**

(A) The chemoenzymatic synthesis of  $^{ss}B43.13-IR800$ ; (B) flow cytometry data illustrating the binding of  $^{ss}B43.13-AF488$  to CA125-positive OVCAR3 human ovarian cancer xenografts. In the blocking experiment, a 75-fold excess of unlabeled  $^{ss}B43.13-AF488$  was employed; (C) fluorescence microscopy images showing CA125-positive OVCAR3 (left) and CA125-negative SKOV3 cells (right) stained with  $^{ss}B43.13-AF488$  and counterstained with DAPI.

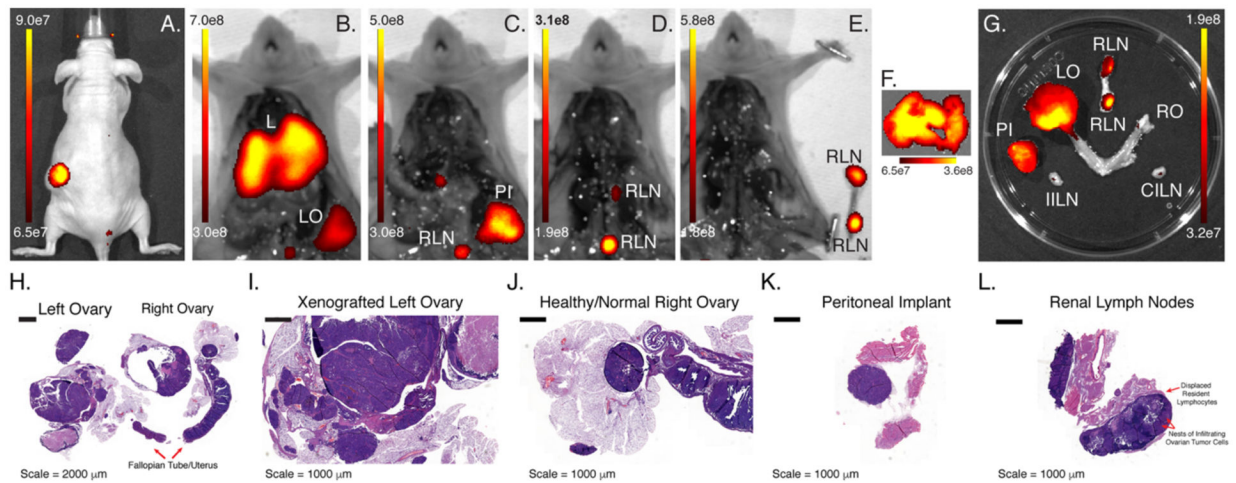


**Figure 2. *In vivo* and *ex vivo* NIRF imaging using <sup>89</sup>Zr-B43.13-IR800.**

(A) NIRF image of a mouse bearing an orthotopic, CA125-positive OVCAR3 xenograft implanted in the left ovary obtained 120 h after the administration of <sup>89</sup>Zr-B43.13-IR800 (100 μg; 0.66 nmol); NIRF images obtained after (B) the exposure of the peritoneal cavity, (C) the removal of the liver [L] and left ovary [LO], (D) the removal of the peritoneal implant [PI], and (E) the removal of the renal lymph nodes [RLN]; *ex vivo* NIRF images obtained of (F) the liver as well as (G) the left ovary, right ovary [RO], renal lymph nodes [RLN], ipsilateral inguinal lymph nodes [IILN] and contralateral inguinal lymph nodes [CILN]; histopathologic analysis of the resected (H) reproductive tract, (I) xenografted left ovary, (J) healthy right ovary, (K) peritoneal implant, and (L) renal lymph nodes

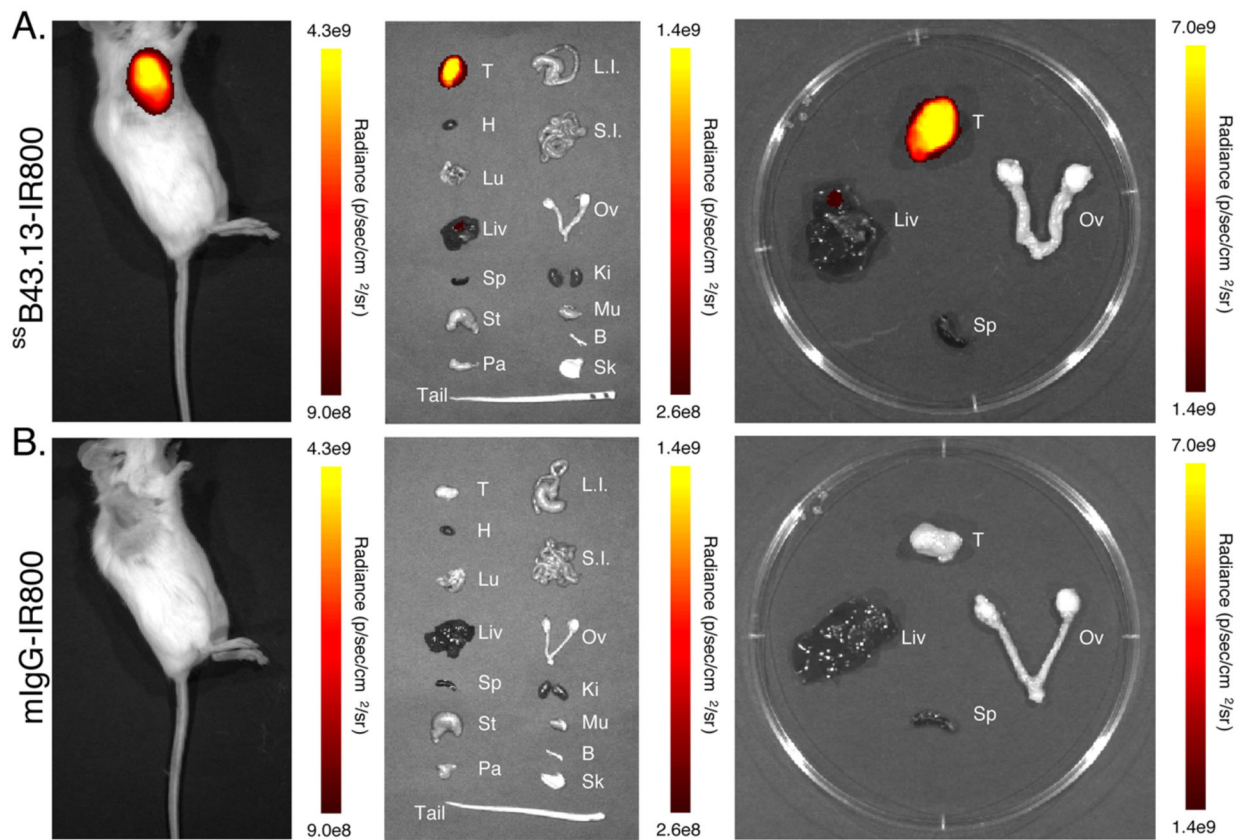


**Figure 3. *In vivo* and *ex vivo* NIRF imaging with  $^{89}\text{Zr}$ B43.13-IR800 and IgG-IR800 in an NSG mouse bearing a subcutaneous OVCAR3 xenograft.**

Representative NIRF images were obtained in an NSG mouse bearing a CA125-positive OVCAR3 human ovarian subcutaneous xenograft 72 hours after the intravenous administration of (A)  $^{89}\text{Zr}$ B43.13-IR800 (50  $\mu\text{g}$ ; 0.33 nmol) and (B) mIgG-IR800 (50  $\mu\text{g}$ ; 0.33 nmol). Upon necropsy, selected organs were harvested, and *ex vivo* NIRF images were obtained: T = tumor; H = heart; Lu = lungs; Liv = liver; Sp = spleen; St = stomach; Pa = pancreas; L.I. = large intestine; S.I. = small intestine; Ov = ovaries; Ki = kidneys; Mu = muscle; Bo = bone; Sk = skin.

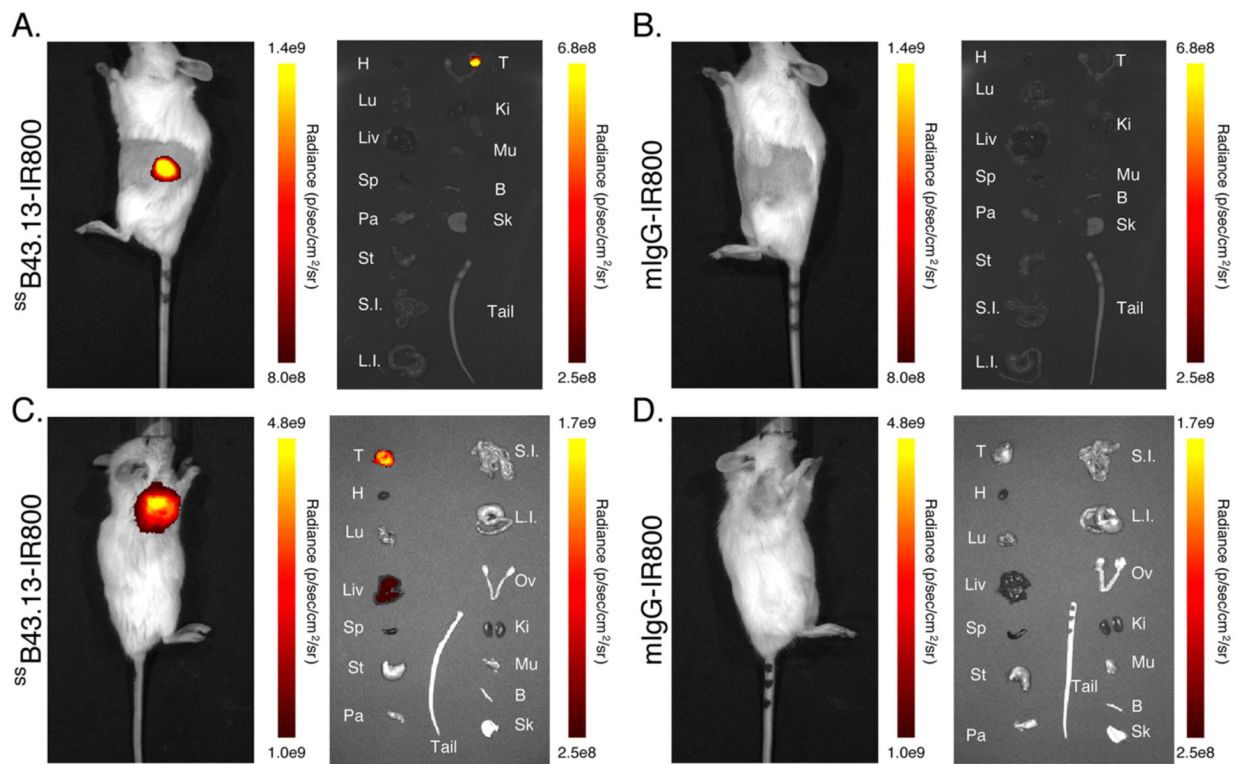


**Figure 4. *In vivo* and *ex vivo* NIRF imaging with <sup>ss</sup>B43.13-IR800 and mIgG-IR800 in NSG mice bearing orthotopic and patient-derived xenografts.**

Representative NIRF images were obtained of (A and B) an NSG mouse bearing a CA125-positive OVCAR3 human ovarian orthotopic xenograft and (C and D) an NSG mouse bearing a CA125-positive patient-derived xenograft acquired 72 hours after the intravenous administration of (A and C) <sup>ss</sup>B43.13-IR800 (50  $\mu$ g; 0.33 nmol) or (B and D) mIgG-IR800 (50  $\mu$ g; 0.33 nmol). Upon necropsy, selected organs were harvested, and *ex vivo* NIRF images were obtained: T = tumor; H = heart; Lu = lungs; Liv = liver; Sp = spleen; St = stomach; Pa = pancreas; L.I. = large intestine; S.I. = small intestine; Ov = ovaries; Ki = kidneys; Mu = muscle; Bo = bone; Sk = skin.

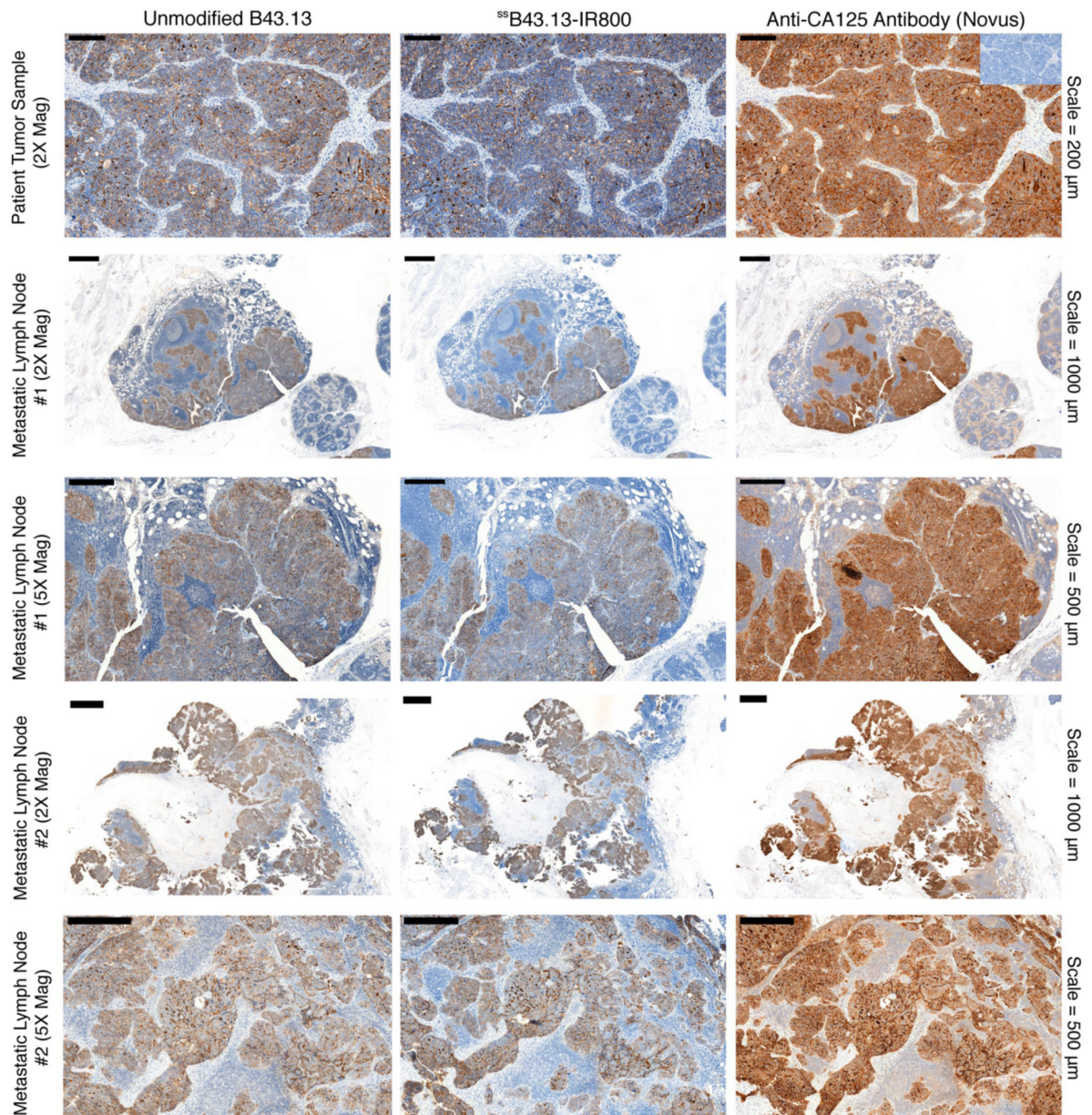


**Figure 5. Histopathologic analysis of tumor and lymph node samples from a patient with metastatic HGSOc.**

Immunohistochemical staining of CA125 in tumor and lymph node samples obtained from a patient who underwent surgical debulking to remove peritoneal tumor masses and metastatic lymph nodes at Memorial Sloan Kettering Cancer Center. The inset image on the top right corner shows staining of the HGSOc tumor section with mouse isotype IgG1 antibody. A high concordance was observed in the staining patterns (brown) when equivalent dilutions of unmodified B43.13, <sup>ss</sup>B43.13-IR800, and a commercially available anti-CA125 antibody (Novus Biologicals, NBP1-96619) were employed for immunohistochemistry. IHC images are representative of samples from 3 independent HGSOc patients.